Non-Native Side Chain IR Probe in Peptides: Ab Initio Computation and 1D and 2D IR Spectral Simulation

Michael L. Zheng,[†] David C. Zheng,[‡] and Jianping Wang*

Beijing National Laboratory for Molecular Sciences, State Key Laboratory of Molecular Reaction Dynamics, Institute of Chemistry, Chinese Academy of Sciences, Beijing 100190, People's Republic of China

Received: December 22, 2009

Infrared frequency region of 2000−2600 cm^{-1} (i.e., ca. 4−5 μm in wavelength) is a well-known open spectral window for peptides and proteins. In this work, six unnatural amino acids (unAAs) were designed to have characteristic absorption bands located in this region. Key chemical groups that served as side chains in these unAAs are C≡C, Phe−C≡C, N═C═O, N═C═S, P−H, and Si−H, respectively. Cysteine (a natural AA having S−H in side chain) was also studied for comparison. The anharmonic vibrational properties, including frequencies, anharmonicities, and intermode couplings, were examined using the density functional theory. Broadband linear infrared (IR) and two-dimensional (2D) IR spectra were simulated for each molecule. It is found that all of the side chain modes have significant overtone diagonal anharmonicities. All have moderate transition dipole strengths except the C≡C and S−H stretching modes, in comparison with the C═O stretching mode. In each case, a collection of 2D IR cross peaks were predicted to appear due to the presence of the side chain groups, whose strengths are closely related to the intramolecular anharmonic interactions, and to the transition dipole strengths of the coupled vibrators. Further, potential energy distribution analysis and high-order anharmonic constant computation showed that these IR probes possess a varying degree of mode localization. The results suggest that these IR probes are potentially useful in complementing the well-studied amide-I mode, to investigate structures and dynamics of peptides and proteins.

1. Introduction

Unnatural amino acids (unAAs) have been an intense research focus in recent years.[1–9] Incorporation of the unAAs into proteins via modern synthetic and biological methods[1–3] can become a powerful tool to investigate structure, dynamics, localization, and biomolecular interactions both in vitro and in vivo.[10] By introducing an unnatural side chain (SC) at the C_α position of an amino acid, novel spectral probes can be produced. For example, unAA-based fluorescent probes[6,10] and infrared (IR) probes[4,5,11–14] have been reported in recent years. For the IR probes, it is the intrinsic vibrational motion that serves as a "chromophore", which can be as simple as a diatomic stretching. Such simple SC groups certainly have the advantage of being small in comparison with typical fluorescent probes, thus having minimal structural perturbation of the polypeptide secondary structure. Further, carefully designed SC groups may have their characteristic IR absorption bands tuned to desired frequency regions so as to avoid spectral overlap with vibrational bands in native amino acids, thus allowing convenient spectral measurements to be carried out.

IR spectroscopy has been a powerful tool to investigate molecular structures because a chemical bond or a functional group in a molecule vibrates at a characteristic frequency or a set of frequencies. As an extension of the traditional IR spectroscopic technique, femtosecond two-dimensional IR (2D IR) is capable of providing direct structural details of molecules in condensed phases with chemical-bond level of structural resolution and ultrafast time resolution.[15–21] 2D IR has been used extensively in revealing structural and dynamic information of secondary structures of biological importance[22–27] because a 2D IR spectrum carries information of intramolecular interaction that is not available from traditional 1D IR spectroscopy. Ideally a collection of 3*N*-6 anharmonic vibrational motions (with *N* being the total number of atoms) and their couplings in a molecule can be used to decipher the three-dimensional (3D) structure of the molecule.[28] However, a well-known limitation of IR spectroscopy is its spectral congestion in commonly occupied frequency regions. In a typical mid-IR spectrum of protein, highly localized stretching vibrations are often located above 2500 cm^{-1} where a large number of delocalized stretching or bending vibrations are crowded below 2000 cm^{-1}. For instance, the well-known amide-I band of polypeptides and protein, being mainly the amide C═O stretching vibration, exists in the frequency region of ca. 1600−1700 cm^{-1}. This band has been well studied for a number of reasons. It is known to have a strong IR absorption cross section and have a well-characterized band profile, which are known to be very sensitive to peptide secondary structures. The vibrational exciton model for this mode[29] has been developed to describe intermode coupling and excitonic band structures upon the action of the coupling. However, because of its intrinsic bandwidth (ca. 10 cm^{-1}), the multiple C═O absorption bands in a multiamide polypeptide system can become largely overlapped; therefore finer structural information is not directly available. Isotope substitution has to be used to shift a particular amide-I site state from the rest of the band in order to probe peptide local structures and dynamics.[22,30–33]

Developing new IR probes for peptide structures and dynamics in a desired spectral region is of great interest. It is for this reason that unAA-based IR probes were designed. Recent IR

* To whom correspondence should be addressed. E-mail: jwang@iccas.ac.cn. Tel: +86-010-62656806. Fax: +86-010-62563167.
[†] Visiting scholar. Current address: Jericho, NY 11753.
[‡] Summer student. Current address: Jericho High School, Jericho, NY 11753-1201.

10.1021/jp912062c
Published on Web 01/21/2010

SCHEME 1: Structure of Alanine-Based Unnatural Amino Acids with R Groups Introduced into the Side Chain

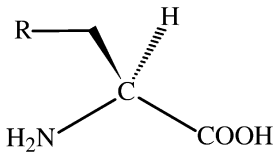

(a) R = −C≡CH, Ala_{CC}; (b) R = −N=C=O, Ala_{NCO}; (c) R = −N=C=S, Ala_{NCS}; (d) R = $-PH_2$, Ala_{PH}; (e) R = $-OSiH_3$, Ala_{SiH}; (f) R = −Phe−C≡CH, Phe_{CC}; (g) R = −SH, Cys. Cysteine was examined for comparison.

studies of biomolecules consisting of functional groups such as nitrile (C≡N),[4,11,12] cyanate (O−C≡N), and thiocynate (S−C≡N)[13] at the SC position have been reported, which all have IR absorption bands falling in the 2000−2600 cm^{-1} (ca. 4−5 μm in wavelength) region. This is a region in which natural AA residues do not have IR absorption bands except cysteine (Cys). The feasibility and usefulness of the above-mentioned chemical groups in revealing peptide local structures and dynamics have been demonstrated in these studies. Similar studies involving the nitrile group have shown to exhibit sensitivity to protein local structure and local solvent electrostatic environment.[5] Further, the 2D IR signature of other chemical groups[12] having IR absorption bands in this region have also been explored very recently.

An in-depth knowledge of anharmonic vibrational properties is key to understanding 2D IR vibrational spectroscopic signatures of molecules. It is widely accepted that inter- and intramolecular interactions, such as hydrogen bonding between functional groups, are essential to the formation of the 3D structure of peptides and proteins.[34] Such interactions may also be responsible for bioreactivity and bioselectivity in biological systems. It is expected that a deeper understanding of such interactions can be obtained through the means of the 2D IR technique. However, even though the studies mentioned above have demonstrated the usefulness of the unnatural SC vibrational modes, the anharmonic behavior of the SC modes is less understood. The characteristics of the 2D IR cross-peaks that may appear due to coupling of the SC mode and the remaining 3*N*-7 modes in a molecule have not been examined. With the aid of the specially designed SC groups, it is expected that the 2D IR study of the unAAs could provide a wealth of information about structures and intramolecular interactions of biological systems.

The goal of this work is to theoretically investigate a group of unAAs with characteristic stretching vibrations whose frequencies are not superimposed by any other vibrational modes in the mid-IR region. For this, six artificial SCs were introduced into the unAAs with an alanine or phenylalanine base, as shown in Scheme 1, namely, Ala_{CC}, Ala_{NCO}, Ala_{NCS}, Ala_{PH}, Ala_{SiH}, and Phe_{CC}. Since among the twenty natural amino acids, Cys is the only one that has a vibrational mode (S−H stretching) located in between the C=O stretching mode and CH_n stretching modes, this AA was also examined in this study for comparison. The thiol group in Cys is also a precursor of the important disulfide bond which is well-known to contribute to the tertiary and quaternary structure. The characteristic IR-active SC stretching modes of ethynyl (−C≡C), isocyanate (−N=C=O), isothiocyanate (−N=C=S), phosphine (PH_2), silane (SiH_3), and thiol (S−H), as well as their couplings with other modes in each molecule were investigated first by quantum mechanical computations. Harmonic and anharmonic vibration frequencies, anharmonicities, as well as transition dipoles were evaluated at the same level of theory. Linear IR and 2D IR spectra were then simulated and vibrational characteristics in the selected regions were examined. The degree of localization of the SC modes was examined through the potential energy distribution (PED) analysis. The force fields behind the diagonal anharmonicity of the SC mode are examined through the anharmonicity composition analysis. Vibrational coupling between the SC mode and the C=O stretching mode are also estimated using electrostatic interaction-based transition dipole coupling (TDC) scheme.

2. Computational Methods

A. Ab Initio Calculations. The anharmonic fundamental, overtone, and combination frequencies of the 3*N*-6 normal modes of the seven model AAs in gas phase were carried out at the level of B3LYP/6-311++G** using Gaussian.[35] Geometries were fully optimized using a tight convergence. A complete set of 3*N*-6 diagonal and off-diagonal anharmonicities was obtained via the second-order vibrational perturbation theory.[36] The fundamental, overtone, and combinational transition anharmonicities of a given mode *i* and a pair of modes *i* and *j* are defined as: $\Delta_i^f = \omega_i - \nu_i$, $\Delta_i^o = 2\nu_i - \nu_{2i}$, and $\Delta_{ij}^c = \nu_i + \nu_j - \nu_{i+j}$ with $i, j = 1, 2, \ldots 3N\text{-}6$, and $i \neq j$. Here ω denotes the harmonic frequency and ν denotes the anharmonic frequency. Details of the calculations were given in a recent study.[37] The Cartesian coordinate-based PED analysis was carried out for each normal mode.

For the *i*th mode, the overtone (diagonal) anharmonicity Δ_i^o is influenced by the interaction between the mode and the remaining 3*N*-7 modes. The contribution from mode *i* itself (local mode contribution) can be conveniently evaluated via the diagonal cubic and quartic anharmonic terms in the potential energy function

$$\delta = -\Phi_{iiii}/8 + 5\Phi_{iii}^2/\omega_i/24 \quad (1)$$

where Φ_{iiii} and Φ_{iii} are the diagonal quartic and cubic force constants of the *i*th mode.

B. Coupling Estimation. The anharmonic vibrational coupling between the C=O and the SC stretching modes in each AA was estimated by using the well-known TDC scheme.[38] The TDC is essentially the potential for the interaction between pairs of dipoles in space. Because the TDC scheme is electrostatic interaction in nature, presumably it can be used to estimate the vibrational coupling between any two vibrational modes. The TDC (in cm^{-1}) is computed by using the following formula

$$\beta_{ij} = (1/\varepsilon)[(\mu_i \cdot \mu_j) - 3(\mu_i \cdot e_{ij})(\mu_j \cdot e_{ij})]/r_{ij}^3 \quad (2)$$

where ε is the dielectric constant (which is assumed to be 1), μ_i is the *i*th transition dipole moment (in $D\text{Å}^{-1}$ $amu^{-1/2}$), r_{ij} is the distance between point dipoles *i* and *j* (in Å), and e_{ij} is the unit vector connecting *i*th and *j*th vibrators. Here the point dipole is set to the center of mass of a given mode. The transition dipole moment, defined as the change of electric dipole moment with respect to the displacement in the nuclear coordinates was calculated using Hessian and atomic polar tensor methodologies at the optimized molecular geometries.

C. Simulations of the Linear and Nonlinear IR Spectra. The ab initio based all-mode computational approach[28] was used to simulate the broadband 1D IR and 2D IR spectra. A brief

description is as follows. Anharmonic fundamental frequencies and the transition dipole moments calculated using the B3LYP functional were used as input for the linear response function in order to simulate the 1D IR spectra. The computed anharmonic frequencies and transition intensities were used directly in 1D IR spectra simulation with spectral line broadened using the line broadening parameters described below. The principle of 2D IR spectroscopy is based on vibrational anharmonicity that fundamentally incorporates higher order interactions from all modes into the potential energy. Anharmonicities of the overtone and combination bands, IR intensities, and spatial angles between the transition dipole moments were used as input to the third order nonlinear response function in order to simulate the 2D IR spectra. Each simulated 2D IR spectrum of (3*N*-6) × (3*N*-6) normal modes includes both the rephasing and nonrephasing 2D IR signals at equal weight, depicting a pure absorptive 2D line shape. This is equivalent to experimentally using a four-wave mixing technique (photon echo) to collect these spectra.[39] Such a 2D spectrum can be regarded as a complete set of intramolecular interactions of the 3*N*-6 vibrations; the off-diagonal peaks represent the anharmonic vibrational interaction of a given pair of vibrators. A Voigt profile was assumed for line broadening with the fwhm for the homogeneous Lorentzian line width and the inhomogeneous Gaussian line width set to 7.5 and 25 cm^{-1}, respectively. For simplicity the same line broadening parameters was assumed for all the 3*N*-6 modes. The lifetime was assumed to be 1 ps for all the modes, to account for the lifetime broadening. Frequency distributions were assumed to be fully correlated. Therefore a typical simulated 2D IR pairwise signal shows a positive and a negative elliptical profile, tilted at 45° angle with an aspect ratio (the ratio of major and minor axis lengths of an ellipse) at nearly 3. It should be pointed out that the parameters given above were used to demonstrate the 1D and 2D IR spectra features. More realistic parameters, once available, can be easily incorporated into the spectral simulation protocols. In addition, although the anharmonic couplings between the SC and the C═O stretching modes were estimated using the TDC schemes in the present study, this coupling scheme was not used in the spectral simulation protocol. Rather, the intermode interactions were expressed as combinational anharmonicities in the 2D IR cross peaks.

The computation of anharmonic frequencies for multiple vibrational modes using the second-order vibrational perturbation theory is known to be quite time-consuming, in particular for large molecules. In this study, the wall-clock time required for the frequency computations are approximately one week except for Phe_{CC} (which is about seven weeks), using a multicore computer server (4-CPU, 3.0 GHz, 4 GB shared memory). The 2D IR simulations take approximately 40 min per molecule per CPU using an in-house written Java program that runs under Linux, which is adopted from an earlier version of code.

3. Results and Discussions

A. Anharmonic Vibrational Characteristics: SC vs C═O. The anharmonic vibrational properties of the seven molecules shown in Scheme 1 with ten IR-active SC stretching modes are examined. Listed in Table 1 are the calculated vibration frequencies (harmonic and anharmonic), and the vibrational band assignment for the characteristic SC stretching mode of each molecule. The ratio of the C═O and the SC stretching transition intensities ($I_{C=O}/I_{SC}$) is also given. Diagonal quartic and cubic anharmonic force constants, anharmonicities, local mode contribution to the overtone anharmonicity, and PED values, are listed in Table 2 for the SC modes and in Table 3 for the C═O modes.

TABLE 1: Mode Assignment, Harmonic (ω) and Anharmonic (ν) Frequencies (in cm^{-1}), and Transition Intensity (in km/mol) of the SC Mode (In Comparison with That of the C═O Stretching) in Each of the unAAs and Cys

species	main vibration[a]	ω	ν	I_{CO}	I_{SC}	I_{CO}/I_{SC}
Ala_{CC}	str	2222.0	2185.1	282.77	3.63	77.90
Ala_{NCO}	asym str	2361.3	2311.4	330.42	1349.30	0.24
Ala_{NCS}	asym str	2159.7	2100.5	373.88	1221.97	0.31
Ala_{PH}	asym str	2390.6	2296.4	330.31	68.36	4.83
	sym str	2366.1	2277.3	330.31	75.24	4.39
Ala_{SiH}	asym str	2281.3	2197.8	273.87	91.13	3.00
	sym str	2222.1	2145.7	273.87	102.89	2.66
	asym str	2216.5	2138.5	273.87	134.66	2.03
Phe_{CC}	str	2201.1	2163.8	291.70	15.70	18.58
Cys	str	2659.4	2545.2	324.90	5.24	62.00

[a] asym = asymmetric; sym = symmetric; str = stretching. Assignment is based on the PED (see Table 2).

TABLE 2: Harmonic Frequency (ω), Diagonal Quartic and Cubic Force Constants (Φ_{iiii} and Φ_{iii}), Fundamental (Δ^f) and Overtone (Δ^o) Diagonal Anharmonicities, Local Mode Contribution (δ) to Δ^o, and the Cartesian Coordinate-Based PED, for the SC Mode in Each of the unAAs and Cys[a]

molecule	ω	Φ_{iiii}	Φ_{iii}	δ	Δ^f	Δ^o	δ/Δ^o	PED
Ala_{CC}	2222.0	122.7	−473.5	65.7	36.9	18.1	0.31	0.44
Ala_{NCO}	2361.3	142.6	−13.9	−17.8	49.8	34.2	--	0.96
Ala_{NCS}	2159.7	156.6	−500.9	4.6	59.2	46.8	0.10	0.94
Ala_{PH}	2390.6	681.6	1358.1	75.5	94.3	79.3	0.95	0.98
	2366.1	696.1	−1366.0	77.3	88.9	79.7	0.97	0.98
Ala_{SiH}	2281.3	585.6	1239.3	67.1	83.6	68.1	0.99	1.00
	2222.1	528.1	−1123.2	52.3	76.4	57.9	0.90	0.92
	2216.5	540.6	1083.2	42.7	78.1	58.3	0.73	0.93
Phe_{CC}	2201.1	124.7	−462.1	4.6	37.3	15.1	0.30	0.46
Cys	2659.4	810.7	−1599.1	99.0	114.2	101.8	0.97	1.00

[a] Units are in cm^{-1} except PED.

TABLE 3: Harmonic Frequency (ω), Diagonal Quartic and Cubic Force Constants (Φ_{iiii} and Φ_{iii}), Fundamental (Δ^f) and Overtone (Δ^o) Diagonal Anharmonicities, Local Mode Contribution (δ) to Δ^o, and the Cartesian Coordinate-Based PED, for the C═O Stretching Mode in Each of the unAAs and Cys[a]

molecule	ω	Φ_{iiii}	Φ_{iii}	δ	Δ^f	Δ^o	δ/Δ^o	PED
Ala_{CC}	1816.1	169.5	−546.5	13.1	33.8	20.4	0.64	0.74
Ala_{NCO}	1834.3	163.3	−532.5	11.8	32.1	20.5	0.58	0.73
Ala_{NCS}	1835.2	169.4	−535.2	11.3	31.1	19.9	0.57	0.74
Ala_{PH}	1833.7	168.6	−534.5	11.4	34.9	18.1	0.63	0.73
Ala_{SiH}	1846.4	178.3	−566.2	13.9	39.3	20.9	0.67	0.81
Phe_{CC}	1809.5	166.7	538.9	12.6	29.8	21.5	0.58	0.70
Cys	1806.3	170.6	548.7	13.4	32.9	22.1	0.62	0.73

[a] Units are in cm^{-1} except PED.

First, it can be seen from Table 1 that both the ω_{SC} and ν_{SC} of each molecule lie in the frequency range between 2100−2660 cm^{-1}; however, each of the AAs has a (or a set of) characteristic SC stretching frequency, of which the transition intensities are apparently mode-dependent. In comparison with the C═O stretching band, very strong IR transitions are predicted for N═C═O and N═C═S side chains, whereas weak transition intensities are predicted for C≡C and S−H stretching modes. A nearly five-time enhancement in the transition intensity is seen in the case of Phe_{CC} in comparison with Ala_{CC}, indicating the role played by the phenyl group. The PH and SiH stretching modes have comparable transition intensities as the C═O modes. It is also interesting to note that the presence of the phenyl ring also causes a red shift in the C≡C stretching frequency.

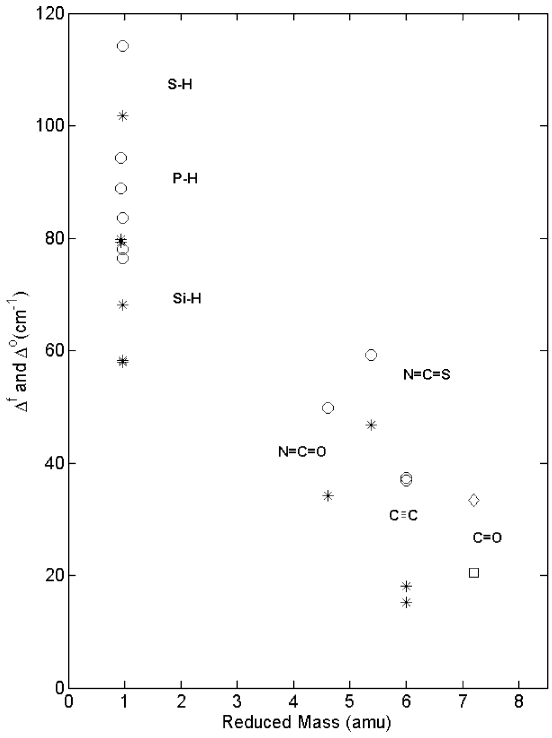

Figure 1. Computed fundamental anharmonicity (circle) and overtone anharmonicity (star) of the SC stretching mode, the averaged fundamental anharmonicity (diamond) and overtone (square) anharmonicity for the C═O stretching mode for the AAs listed in Scheme 1, plotted as a function of the reduced mass.

Second, as shown in Table 2, the anharmonic corrections are quite substantial for the SC stretching modes. The fundamental anharmonicity (Δ^f) varies from 36.9 to 114.2 cm^{-1}. Similar trend from 15.1 to 101.8 cm^{-1} can also be observed in overtone anharmonicities (Δ^o). Since Δ^o is a direct 2D IR diagonal observable, it shall be measurable in the 2D IR spectrum of the SC stretching mode. As a comparison, the average anharmonicity of the fundamental and overtone C═O stretching mode of all the model molecules are found to be 33.4 and 20.5 cm^{-1} (Δ^f, Δ^o in Table 3), which is consistent with a recent study[37] where the anharmonic parameters were predicted for the amide modes at various level of theories. Shown in Figure 1 are the computed fundamental and overtone anharmonicities versus the reduced masses for the SC modes in the unAAs listed in Scheme 1. Also shown are the averaged fundamental and overtone anharmonicities of the C═O modes. It is obvious that the SC modes have small "effective" masses and large anharmonicities in comparison with the C═O mode, and the anharmonicities are both species- and reduced-mass dependent. The extent of anharmonic corrections is determined by the contributions of cubic and quartic terms of the Taylor expansion of the potential energy function. In a classical picture, the harmonic assumption is no longer valid when the nuclei displacement is large, therefore stretching modes involving H atom, which is the lightest in mass, tend to be more anharmonic, thus having larger anharmonicity. This is the case for the SH, PH, and SiH stretching modes.

Third, it is interesting to examine factors that determine the overall magnitude of the overtone anharmonicity (Δ^o) of the SC modes. It is well-known that the diagonal anharmonicity of a given mode depends on not only the mode itself, but also other modes with which it is coupled.[40] The local mode contribution from mode i was computed using eq 1 and the results were listed in Table 2 for all the SC modes. A similar analysis for the C═O stretching modes is given in Table 3. It is seen that the δ term in eq 1 contributes significantly to Δ^o in several SC cases in Table 2, suggesting their localized nature. For this reason, the ratio δ/Δ^o may serve as a measure of mode localization if δ and Δ^o have the same sign. However, in the case of Ala_{CC}, Ala_{NCO}, Ala_{NCS}, and Phe_{CC} large difference between δ and Δ^o exist. This is because δ is only one part of Δ^o; the other part contributing to Δ^o comes from the cross terms in the form of $\sum_{k\neq i}^{3N-7}\Phi_{iik}^2(8\omega_i^2 - 3\omega_k^2)/(4\omega_i^2 - \omega_k^2)/\omega_k/8$,[37] where Φ_{iik} is the semidiagonal cubic force constant and ω_k is the harmonic frequency of mode k ($k \neq i$). For example, the negative δ for NCO can be compensated by this term and it is found that the symmetric stretching NCO (with $\Phi_{iik} = 416.2$ cm^{-1} and $\omega_k = 1481.1$ cm^{-1}) contributes 27.6 cm^{-1} to the Δ^o of the asymmetric NCO stretching mode shown in Table 2. This suggests that the Δ^o of the NCO asymmetric stretching mode is also sensitive to the intermode interactions. This is actually an intrinsic property of any delocalized normal mode. On the other hand, the same analysis reveals that, in the case of the C═O stretching mode, the δ/Δ^o ratio is in the range of 0.57−0.67. In other words, the C═O modes are just about 60% localized according to this measure, where the SC modes demonstrate a varying degree of local mode contributions.

Fourth, the Cartesian coordinate-based PED of the SC modes shown in Table 2 represents the contribution of nuclei displacement from the atoms in the SC groups. Similar analysis for the C═O mode is shown in Table 3. The PED is a measure of the degree of "through-bond" contribution from a submolecular group to a specific normal mode, therefore a "true" measure of the mode localization. It is well-known that the C═O stretching motion contributes significantly to the amide-I normal mode in peptides, and the nearby nuclei motions have an insignificant impact. The partially delocalized nature of the amide-I mode is believed to be sensitive to local backbone and solvent environment.[22] The average PED value of the C═O vibrational mode of the molecules selected in the current work is found to be 0.74 (Table 3), which is in agreement with the nature of the C═O stretching mode in these AAs. However, the PED values of the characteristic SC stretching modes of the seven AAs are quite different, which indicate different degrees of localization of the SC groups. For example, for the Ala_{SiH} group, the three SiH stretching modes are highly localized with PED values ranging from 0.92 to 1.0. There is also a subtle difference in their PEDs: each of the two low-frequency modes is localized on one of the two SiH bonds (PED $\sim$ 0.93 vs 0.07), while the high-frequency mode is almost entirely localized on the other SiH bond (PED $\sim$ 1.00). Therefore, sitting on the same SC and having transition dipole strength comparable to that of the C═O stretching mode in peptides as shown below, each of the three SiH stretching mode can potentially be utilized to sense subtle structural or environmental variations in the neighborhood.

Further, it can be observed in Table 2 that the PED values of the SC modes can be in general classified into two groups, one around 0.45 (for Ala_{CC} and Phe_{CC}), and the other around 0.92−1.00 (for the rest of modes), which can be potentially useful to report local, regional, and global structural information. This is complementary to the existing probe of the C═O stretching mode which is only partially delocalized. Furthermore, the agreement between PED and δ/Δ^o is well demonstrated in the case of the C═O stretching modes (Table 3), even though the δ/Δ^o values are generally lower in certain degrees. This is because the PED and δ/Δ^o reflect different aspects of the mode localization. The ratio δ/Δ^o is actually a measure of how much the anharmonic shift of the overtone state energy is controlled

by the diagonal terms of the anharmonic potential. Such a shift is determined by the anharmonic force fields of the molecular system. PED is a measure of the vibrational wave functions for the atoms of interest that contributes to a given delocalized normal mode. A completely localized mode even though being rarely seen, shall have PED equal to unity.

Lastly, the unique vibrational properties of the SC modes are further examined here. (1) The C≡C stretching mode. This mode exists in both ethynyl-derived amino acids, Ala_{CC} and Phe_{CC}, of our model molecules with an absorption band at 2185.1 and 2163.8 cm^{-1}, respectively (Table 1). However, the PED analysis shows that the triple carbon−carbon bond stretching contributes to only about 45% of the mode. One major factor influencing the mode is the terminal hydrogen atom which accounts for another ca. 53% of the PED. This means that this IR probe may be used to report the hydrophobic environment of this SC group. This can be done experimentally by examining the frequency distribution and line shape of the C≡C stretching mode, which will be influenced by intramolecular as well as solvent−solute interactions. The relatively low transition dipole strength seems to be a disadvantage of the C≡C group, however, this mode can still be a potentially useful vibrational probe due to the presence of significant cross-peaks associated with this mode, and also to its unique frequency location. Further, an almost pure stretching mode for the ≡C−H group can be located at 3347.5 and 3348.7 cm^{-1} for the two molecules respectively with a PED value above 0.98. This suggests that the ≡C−H stretching mode may serve as a local structural probe. (2) The N═C═O and N═C═S asymmetric stretching modes. The molecular structures of N═C═O and N═C═S groups are similar in that the center carbon atom shares a double bond with each of the other atoms forming a linear triatomic group. The symmetric stretching motion can be found at 1459.0 and 738.7 cm^{-1}, respectively; however, their absorption strengths are typically weak due to the symmetric charge redistribution during the vibrational motion. The signature absorption peaks of the N═C═O and the N═C═S groups are the asymmetric stretching motions at 2311.4 and 2100.5 cm^{-1} (Table 1). The two modes are mostly localized with high PED values. The unique feature of this probe is its large IR absorption cross section (Table 1). The transition intensity is near three times as large as that of the average carbonyl (C═O), thus making the group an excellent probe in 2D IR experiments, especially suitable to detect weak molecular couplings. (3) The S−H stretching mode. The S−H stretching mode is found at 2545.2 cm^{-1} and is entirely localized with a unity PED. The group is similar to N−H stretching in peptides[37] with a high degree of localization, but unlike the N−H group which has a larger electronegativity difference, the thiol group rarely involves in hydrogen bonding. As shown in Table 2, the anharmonicities of the fundamental and overtone are the largest among the model molecules selected in the current study (114.2 and 101.8 cm^{-1}, respectively). (4) The PH_2 and SiH_3 group. These two groups consist more than one bond with the hydrogen atom, therefore the linear IR spectra show multiple symmetric and asymmetric stretching modes around the spectral region interested. As can be seen in Table 1, the stretching mode is relatively close to each other within 20 cm^{-1} for the phosphine and 60 cm^{-1} for the silane group with reasonable dipole derivatives. They are all highly localized with a PED value >0.92. Their anharmonicities are relatively large among the group of model molecules investigated.

B. Intermode Coupling. Intermode coupling between the SC stretching modes and the nearby C═O stretching mode in each AA is examined (Table 4). It is well-known that vibrational modes are coupled to one another, either through covalent bond or through space. What one observes experimentally by FTIR spectrometer is a picture after vibrational coupling (the normal mode picture). The total anharmonic coupling strength of the SC and CO modes is reflected in the magnitude of the combinational anharmonicity$\Delta^{\S}_{SC,CO}$, which is determined, similarly as the overtone anharmonicity discussed above, by the quartic and cubic force anharmonic constants. The computed small anharmonicities here (less than 1 cm^{-1} except for the first three cases in Table 4) suggest that the intermode coupling is in a weak coupling regime. In addition, the intermode distance, defined as the distance between two centers of mass in the two corresponding modes, is found to range from 3.5 to 7.0 Å in these AAs as shown in Table 4. This is in the range where the through-space electrostatic interaction begins to dominate the intermode coupling. For this reason we have attempted to utilize the TDC scheme for a quick assessment of the coupling.

TABLE 4: Transition Dipoles of the SC Mode and the C═O Stretching Mode ($|\mu|$ in $DÅ^{-1}$ $amu^{-1/2}$), Point Dipole Distance between Two Modes (r, in Å), Angle between the Two Dipole (θ, in degree), Computed TDC (β, in cm^{-1}), in Comparison with the Combinational Anharmonicity ($\Delta^{\S}_{SC,CO}$, in cm^{-1}) in Each of the unAAs and Cys

species	$\lvert\mu_{SC}\rvert$	$\lvert\mu_{CO}\rvert$	θ	r[a]	$\beta_{SC,CO}$	$\Delta^{\S}_{SC,CO}$
Ala_{CC}	0.29	2.59	77.1	3.5	0.4	1.4
Ala_{NCO}	5.65	2.80	84.5	5.1	1.5	3.9
Ala_{NCS}	5.38	2.97	35.4	5.6	−0.2	4.1
Ala_{PH}	1.27	2.80	65.5	4.5	1.8	−0.6
	1.33	2.80	34.8	4.5	0.2	−0.5
Ala_{SiH}	1.47	2.55	129.9	4.9	−1.3	0.0
	1.56	2.55	133.0	4.9	1.1	−0.1
	1.79	2.55	116.8	4.9	−0.2	0.0
Phe_{CC}	0.61	2.63	105.9	7.0	−0.1	0.8
Cys	0.35	2.77	41.9	4.6	−0.4	0.9

[a] Distance between center of mass of the two modes.

We first examine the transition dipoles of the SC and C═O stretching modes. In Table 4 the computed transition dipoles of the C═O stretching modes are consistent from molecule to molecule. The average $|\mu_{CO}|$ is found to be 2.70 $DÅ^{-1}$ $amu^{-1/2}$, which is similar to that of the amide-I mode in an isolated peptide unit.[41] Certain SC modes, for example, the C≡C and S−H stretching modes in Ala_{CC} and Cys have relatively smaller dipole magnitude (0.29 and 0.35 $DÅ^{-1}$ $amu^{-1/2}$, respectively) where the NCO has the largest (5.65 $DÅ^{-1}$ $amu^{-1/2}$), and the latter is more than double that of the C═O modes. Here the magnitude of the transition dipole is related to the charge redistribution during nuclei motions associated with a specific vibration mode. For example, in the asymmetric stretching of NCO the carbon atom is oscillating between the relatively static N and O atoms, which causes a large charge shift; where in the symmetric stretching mode, the carbon atom is relatively static but the N and O atoms move out-of-phase with regard to the carbon atom. The charge distribution in this case is not altered as much as that of the asymmetric stretching mode.

The computed TDC values between the SC modes and the C═O stretching modes ($\beta_{SC,CO}$) are generally quite small (Table 4). The largest coupling is seen in the case of Ala_{NCO}, and the smallest coupling is seen in Phe_{CC}. These couplings shown in Table 4 are also found to correlate roughly with the absolute values of the combinational anharmonicities $\Delta^{\S}_{SC,CO}$, having a correlation coefficient of 0.23. This is probably because the SC and the C═O species are three-bond away from each other. Further, for largely separated vibrators such as the C═O and

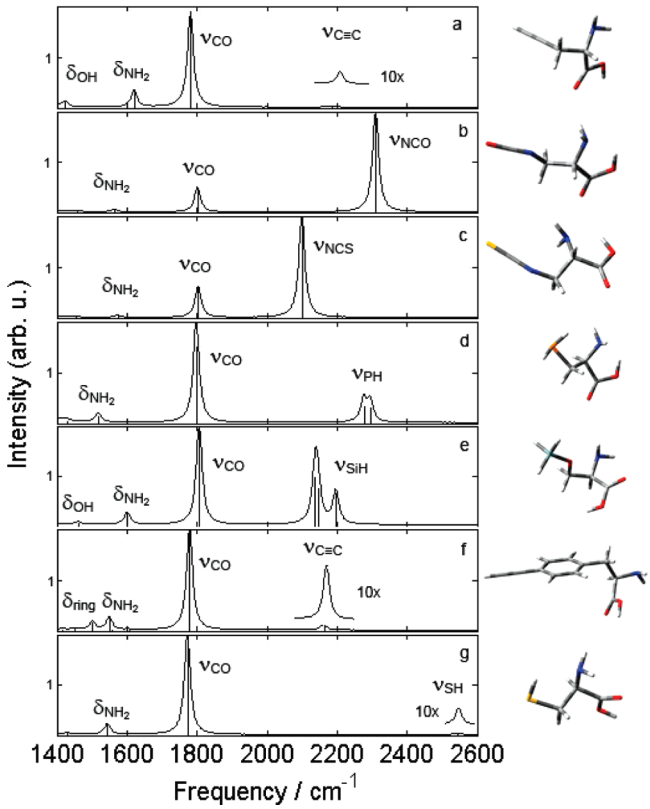

Figure 2. Simulated linear IR spectra and optimized geometries of the unAAs and Cys in the region of 1400−2600 cm^{-1} with major band assignments. (a) Ala_{CC}; (b) Ala_{NCO}; (c) Ala_{NCS}; (d) Ala_{PH}; (e) Ala_{SiH}; (f) Phe_{CC}; (g) Cys. Peak intensities of C≡C and SH stretching mode in Ala_{CC}, Phe_{CC}, Cys are enlarged by 10 times as shown within the subplot. Anharmonic frequencies are used. Band assignment is based on PED analysis (see text for details).

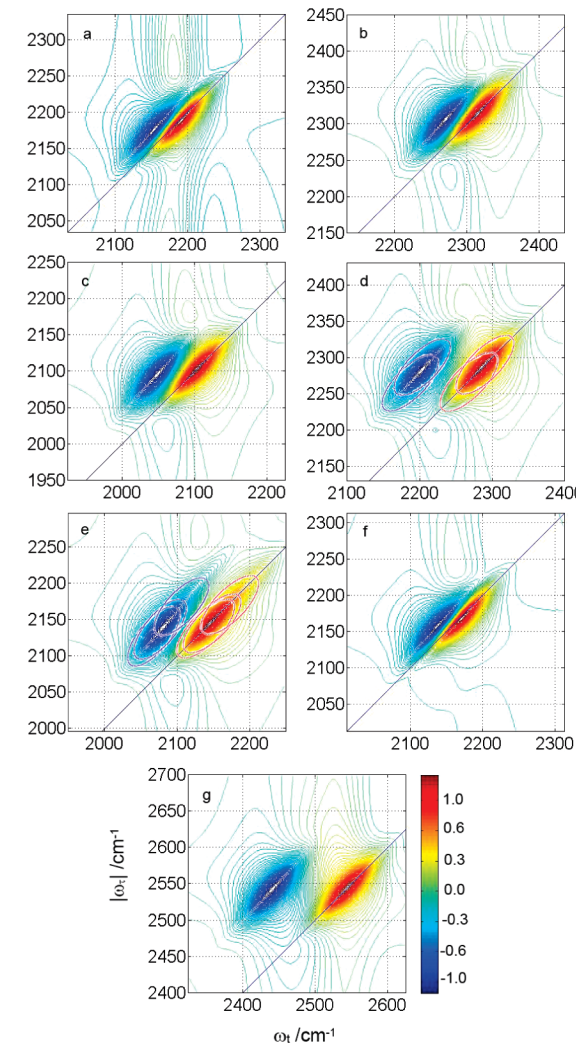

Figure 3. Simulated 2D IR diagonal peaks of the characteristic SC stretching mode of the unAAs and Cys in a spectral area of 300 cm^{-1} × 300 cm^{-1}. (a) Ala_{CC}; (b) Ala_{NCO}; (c) Ala_{NCS}; (d) Ala_{PH}; (e) Ala_{SiH}; (f) Phe_{CC}; (g) Cys. Panels d and e are superimposed by two and three pairs of peaks indicated by ovals, respectively. Spectral intensities are normalized for all panels.

SC stretching modes, such a weak coupling will cause insignificant frequency separation and intensity transfer between the two modes.

C. Linear IR Spectra. The simulated linear IR absorption bands in the region between 1400 and 2600 cm^{-1} (anharmonic frequency basis) of each model molecule are shown in Figure 2. The optimized molecular structures are also given by the side of each panel. This frequency region includes mainly the C═O stretching (ν_{CO}), C−N stretching (ν_{CN}), NH_2 in-plane bending (δ_{NH_2}), OH in-plane bending (δ_{OH}), and most importantly the SC stretching mode (ν_{SC}). The C═O stretching absorption in each case is found to be around 1800 cm^{-1}, which is typical for −COOH group in gas phase. The SC stretching frequencies are found to be in the frequency range between 2100−2550 cm^{-1}. The simulated IR bands for the N═C═O and N═C═S modes are much stronger than that of their C═O modes in panels b and c. However, weak IR bands are shown for C≡C and S−H stretchings modes. For the latter, the absorption peaks have been enlarged by 10 times in Figure 2 for clarity. This picture is consistent with the magnitudes of the calculated transition dipoles in Table 4. Further, Figure 2 also reveals that the triatomic N═C═O and N═C═S groups show similar IR absorption strength that is due to their similarly conjugated linear configuration. Their asymmetric stretching motions show very strong absorptions around 2100−2300 cm^{-1} region because the motion of the central carbon atom causes a large degree of charge redistribution thus a strong transition dipole. The diatomic C≡C and S−H groups have a single absorption peak from their stretching motions. The PH_2 and SiH_3 are nonlinear atomic groups and both the symmetric and asymmetric motions simultaneously involving all hydrogen atoms have strong enough dipole changes that both the motions can be seen in the frequency range. Furthermore, the spectra in Figure 2 clearly demonstrate that the infrared absorption of the characteristic SC stretching modes are located in a spectral region that are not overlapped with normal modes from other parts of the molecules. For the triatomic molecular group NCO and NCS, there also exist bending and symmetric stretching motions, whose anharmonic frequencies are located at 1459.0 and 480.2 cm^{-1}, respectively, with much weaker dipole strength, and the latter is not in the frequency range of Figure 2.

D. 2D IR Spectra of the SC Groups in the Diagonal Region. Frequency- and anharmonicity dependent 2D IR profiles are predicted for the diagonal signals of the SC modes. Shown in Figure 3 are the diagonal peaks of the characteristic stretching modes of C≡C, N═C═O, N═C═S, P−H, Si−H and S−H in each model AA. Each subplot is in a 300 cm^{-1} × 300 cm^{-1} range, which is centered around their anharmonic stretching frequency for best viewing. Here the two frequencies are ω_τ (due to coherence time) and ω_t (due to probing time), respectively.[15] Positive diagonal anharmonicity yields commonly seen 2D IR diagonal peak profiles in all case. The predicted 2D signal

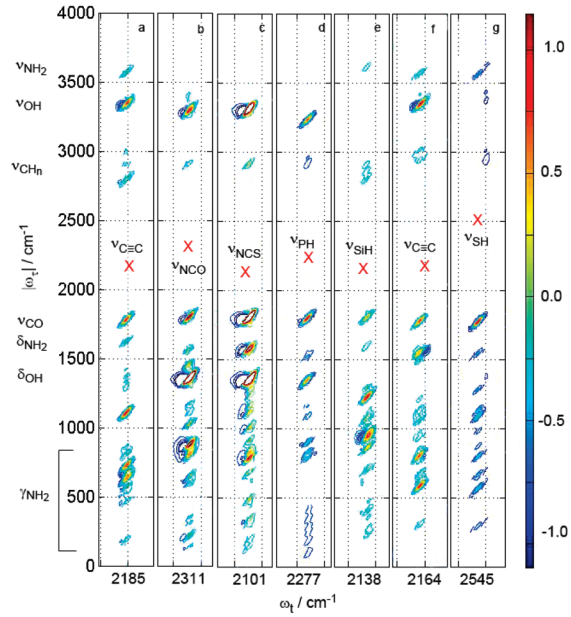

Figure 4. Simulated 2D IR cross peaks between the characteristic SC stretching mode and all other normal modes for each molecule in a range of 0−4000 cm^{-1}. (a) Ala_{CC}; (b) Ala_{NCO}; (c) Ala_{NCS}; (d) Ala_{PH}; (e) Ala_{SiH}; (f) Phe_{CC}; (g) Cys. Red X's indicate the positions of the diagonal peaks of the characteristic stretching modes. The anharmonic frequency of each stretching mode is indicated on the *x*-axis in each subplot. Major band assignment (on the left side) is based on the PED analysis. Spectral intensities are normalized for all panels.

of Ala_{CC} and Phe_{CC} mainly differ by frequency. A 3 cm^{-1} anharmonicity difference does not cause a significant spectral difference in panels a and f. The 2D IR diagonal signals of NCO and NCS are similar except the stretching frequency is lowered by about 200 cm^{-1} for the NCS group. From these 2D IR peaks, it is clearly evident that the S−H stretching has the largest anharmonicity where the C≡C stretching in Phe_{CC} has the smallest. It is interesting to see in subplot (d) and (e) that both the PH_2 and SiH_3 groups involve multiple stretching vibrations as can be seen in the linear IR spectra given above, while the 2D IR shows apparently multiple pairs of peaks. The two P−H stretching modes are 19.1 cm^{-1} apart from each other in frequency, but the anharmonicity of each mode is around 97 cm^{-1}, which is much larger than the frequency difference between each individual mode, therefore pairs of peaks are on top of each other rather than canceling each other. It is similar for the SiH_3 group but the peaks are somewhat extended toward the upper right corner; this is because, as Table 1 shows, that the highest frequency among the three stretching modes is relatively farther away from the other two and has a weaker transition dipole. Solid ovals are placed in the subplots to indicate the individual peaks of the overlapping 2D peaks. The 2D IR spectral characteristics of the SC modes are further discussed below along with their cross peaks with other modes.

E. 2D IR Characteristics of the Intramolecular Interactions Involving the SC Groups. The common feature of the selected SC modes is the nonoverlapping nature of the characteristic stretching mode frequencies, all of which are in the mid-IR range and can be readily accessible by 2D IR experiments at the 4−5 μm wavelengths. Here we focus on each SC group and investigate its coupling-resulted cross-peaks with the rest of the molecule and thus the pros and cons of being a new vibrational marker. Figure 4 shows regional 2D IR spectra of the molecules studied in this work. The 2D IR spectra given here clearly reveal a set of cross peaks between characteristic stretching modes and the rest of the normal modes in each molecule. Figure 5 depicts the computed combinational anharmonicities between the SC modes and the remaining 3*N*-7 normal modes in the seven AAs. These anharmonicities form the basis of the 2D IR cross peaks shown in Figure 4. The mode-dependent and hence structural-dependent anharmonic coupling terms can be seen more easily in this figure. In Figure 4, strong diagonal peaks of the SC groups' characteristic stretching modes are reduced to a symbolic red X in the simulation to reveal weak off-diagonal peaks and also to alleviate apparent spectral congestion. It can be seen that the region around the diagonal peaks of the SC modes is spectrally uncongested in both ω_τ and ω_t dimensions, this again demonstrates our first idea of utilizing these groups as "neat" IR probes.

There are several immediate observations from the 2D IR contour plots shown in Figure 4. The first observation is that the 2D IR strips are reminiscent of the linear IR spectra in that the region below 1500 cm^{-1} shows massive interactions between the characteristic stretching mode and various bending modes. The second observation is that the cross-peaks involving the C═O stretching mode are a clearly seen feature in all cases. The strength of the cross peaks are due to the intermode interactions shown in Table 4. The third observation is that there are other coupled modes with spectral cleanness. For example, cross peaks involving either the C_α−H stretching mode around 2500−3000 cm^{-1} region or the NH_2 in-plane bending just below 1500 cm^{-1} also show a well-defined profile and could become detectable in such broadband 2D IR spectra. The fourth observation is 2D IR cross peaks involving weak IR bands such as C≡C and S−H are also quite substantial, thus allowing intermode interactions to be studied between strong and weak transitions. On the other hand, because the transition dipole strengths of C≡C and S−H stretching modes examined in this study are much smaller than that of the C═O stretching mode, linear IR spectroscopic probe utilizing such vibrations would have been difficult should they be located in a congested spectral area. The results shown in Figure 2 and 4 suggest that such weak transitions can be examined by 2D IR experiments not only because they are background-free, but also because the 2D IR technique is known to be more sensitive than 1D IRs; the 2D IR signal is proportional to the fourth power of the transition dipole,[42] whereas the 1D IR signal is proportional to the square of the transition dipole. Further, upon the availability of broadband IR laser technology, or using tunable two-color 2D IR technique,[43,44] couplings between remote transitions can provide another dimension of experimental choices instead of being limited to the characteristic stretching modes using the traditional IR methodology.

However, since a 2D IR cross-peak signal strength is proportional to the geometric average of the IR cross sections of a pair of coupled vibrators and their combinational band anharmonicity,[45] smaller coupling may still result in reasonable cross peaks (as shown in the following section), if one of the vibrators had reasonable transition dipole strength. This is exactly the case for the cross-peaks between the SC modes and the C═O stretching modes. In all cases, the computed cross-peaks between the SC and the C═O modes show reasonable peak intensities (Figure 4). The profile of the cross peaks, including their orientations and shapes, reflects the joint frequency distributions of the two coupled modes (and hence two chemical species). Thus the presence of the significant cross peaks still makes the weak SC mode a useful structural probe. For this reason, generally speaking even a weak mode is still

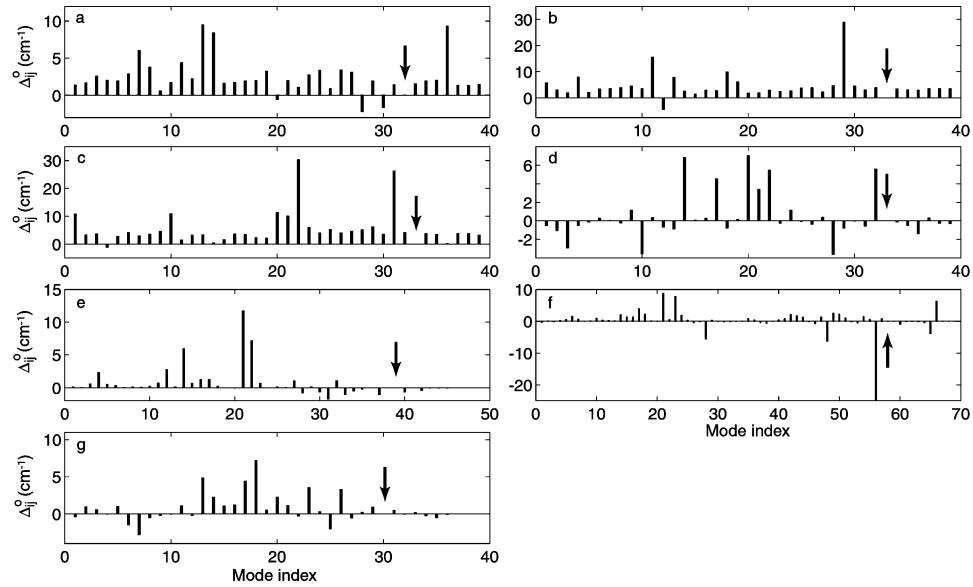

Figure 5. Computed combinational anharmonicities between the SC mode and the remaining $3N$-7 normal modes in each of the AAs. (a) Ala_{CC}; (b) Ala_{NCO}; (c) Ala_{NCS}; (d) Ala_{PH}, high-frequency SC mode only; (e) Ala_{SiH}, high-frequency SC mode only; (f) Phe_{CC}; (g) Cys. Mode frequency renders from low to high. Arrow denotes the SC mode.

useful one way or another in reporting molecular structures and dynamics using 2D IR spectroscopy.

F. The Aromatic Ring Mode. The other unique group worth mentioning in the present study in Phe_{CC} is the phenyl ring. As discussed earlier, the presence of this group also enhances the transition dipole magnitude of the C≡C stretching mode by a factor of 2 (see Tables 1 and 4). Aromatic ring structures are very common in biosystems.[46] The phenyl ring is believed to be negatively charged axially and positively charged equatorially.[46] The hydrogen atom (N−H) on the amino group is positively charged and preferably interacts with the aromatic ring axially.[46] This spatial preference plays an important role in stabilizing protein tertiary structure as shown by Fabian et al.[47] investigating the ring breathing (mainly δ_{CH} and C═C stretching motions) of Phe at 1498 cm^{-1}. The same mode in the Phe_{CC} is found at 1502.1 cm^{-1} in this work. It can be seen from Figure 2 that this mode is clearly visible with reasonable dipole strength. The mode is mainly localized with a PED value of 0.99.

The 2D IR spectrum of the phenyl ring vibration in Phe_{CC} shows interesting patterns. We explore the signature of the modes in detail here. Figure 6 shows the cross peaks of the aromatic ring's breathing mode (1502.1 cm^{-1}, mode 53), with four different C−H stretching modes on the ring (modes 62, 63, 64, and 65 at 3016.7, 3017.0, 3071.4, and 3058.2 cm^{-1}, respectively). It also shows the schematic of the in-pane bending motions. Mode 62 and mode 63 are asymmetric stretching of two hydrogen atoms both of which are on the same side of the ring, while the other two hydrogen atoms do not move. Mode 64 and 65 are asymmetric and symmetric stretching of all four hydrogen atoms. The 2D IR in the region of 1500 and 3050 cm^{-1} mainly shows an aggregate pattern of four cross peaks. The two stretching modes involving just two hydrogen atoms have a positive anharmonicity of 9.8 and 19.9 cm^{-1} (mode 62, 63), where the stretching modes involving four hydrogen atoms have a negative anharmonicity of −8.9 and −10.7 cm^{-1} (mode 64 and 65), therefore the positive (red) and negative (blue) pairs of the 2D IR appear opposite due to the opposite sign of the anharmonicities and some cancellations occur. The cross peak at 2956.7 and 1502.7 cm^{-1} comes from the CH_2 stretching mode (mode 61). The pairwise pattern can be hardly seen because

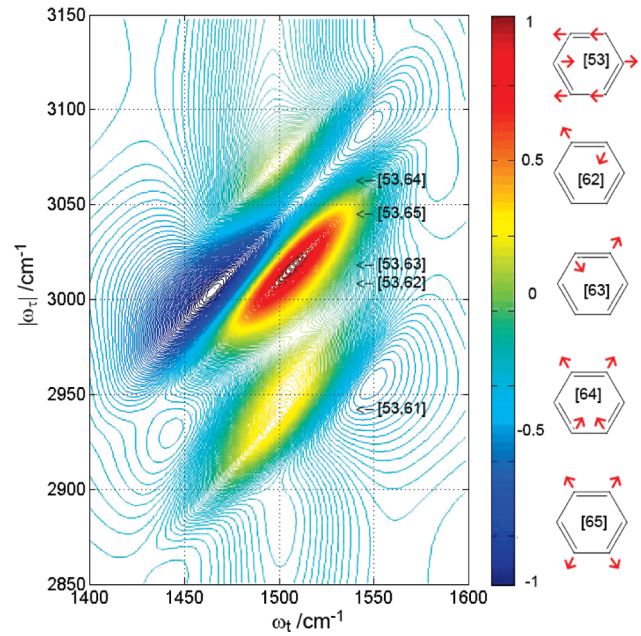

Figure 6. 2D IR signature of aromatic cross peaks of the Phe_{CC} between the ring breathing motion (containing the C−H in-plane bending δ_{CH}) [53] at 1502.1 cm^{-1} and the four C−H stretching modes [62, 63, 64, and 65] at 3016.7, 3017.0, 3071.4, and 3058.2 cm^{-1}, respectively. A weak cross peak at 2956.7 and 1502.1 cm^{-1} is due to the coupling of CH_2 stretching and the ring motion. The schematics of ring motions are on the right side labeled with mode numbers. The anharmonicities for the cross peaks are: $\Delta^c_{53,61} = -1.7$, $\Delta^c_{53,62} = 9.8$, $\Delta^c_{53,63} = 19.9$, $\Delta^c_{53,64} = -8.9$, $\Delta^c_{53,65} = -10.7$ cm^{-1}.

the cross anharmonicity with the breathing mode (mode 53) is only −1.7 cm^{-1}, therefore the red and blue peaks are almost on top of each other and appear as one combined bump. This cluster of cross peaks can be useful in examining the local structural dynamics of the aromatic ring during a biomolecular process as it is affected by both the C═C stretching motion as well as C−H bendings. However, care should be taken for these ring modes because their frequencies may overlap with those of the C−N stretching and N−H in-plane bending modes in the same spectral region.

4. Concluding Remarks

Six non-native amino acids with specially designed SC groups were proposed as novel IR probes for peptide structures in this theoretical work. Cysteine was also chosen in comparison because it possesses the S−H group in its side chain. Quantum mechanical calculations were carried out to evaluate their vibrational characteristics. Potential energy distribution and high-order anharmonic constants were utilized to measure the degree of mode localization of each SC group. Simulated linear IR and nonlinear 2D IR spectra were presented. All of the SC groups show absorption peaks in the region of 2100−2660 cm^{-1} with superb spectral cleanness, allowing a unique spectral characterization of structures of peptides that is not available from the C═O stretching mode.

The results show that these IR probes may be able to sense a wider degree of localization to explore the intramolecular interactions in addition to the intensely focused C═O stretching mode. Ala_{CC} and Phe_{CC} both have a C≡C stretching mode that is about 45% localized on the ethynyl group. This compares to the 74% localization of the C═O stretching mode that is more sensitive to the local chemical environment. The results suggest that the ethynyl group can be instead used as a regional structural probe that is more sensitive to its environment than the C═O stretching mode. On the other hand, the NCO and NCS groups have a localization degree of about 95%, thus they are suited for mostly local structural probes. The thiol, phosphine, and silane groups form the last set of vibrational probes in that they are almost purely local probes with no participation from any other modes in the molecule.

As reflected in the combinational anharmonicity $\Delta^{c}_{SC,CO}$, interaction via high-order force constants are shown to be nonsubstantial between the SC mode and backbone C═O stretching mode in each molecule, indicating weak intermode couplings. Such weak couplings will not significantly affect the diagonal peak intensity of either the SC or the C═O mode, but will cause new cross-peaks. This is because the 2D IR cross-peak signal strength is related to a geometric average of the transition dipole strengths of coupled vibrators. TDC is found to be small and the values are in rough correlation with the magnitude of the combinational anharmonicity.

Further, all the SC modes are predicted to have moderate transition dipole strengths except the C≡C and S−H modes. In particular, the NCO and NCS modes have quite strong IR transition dipole strengths, which are nearly three times of that of a typical C═O stretching mode, showing promise for useful IR probes to be developed for peptide structures. This may also facilitate experimentally probing much weaker cross interactions. The phosphine and silane group both have strong dipole strengths, and both have multiple absorption peaks in the frequency region investigated. In addition, even though the thiol group and the ethynyl group have relatively weaker IR transitions, the background-free spectral location and the enhanced signal sensitivity inherent from the 2D IR methodology would make them experimentally useful. Further, an aromatic ring mode around 1500 cm^{-1} studied here demonstrates that due to the unique axial and equatorial charge distribution of the phenyl structure the aromatic ring mode may serve as a potential vibrational probe for peptide local structures as well.

Furthermore, a group of the SC modes coexisting in a single AA may exhibit some unique features. For example, the collection of three SiH stretching modes can be regarded together as a structural reporter capable of detecting various local environment with transition dipole strength comparable to that of the C═O stretching mode in peptides. Novel SC groups as such shall be potentially useful in revealing molecular structures and dynamics, once incorporated into polypeptides and proteins. It is less likely that small SC groups as such would cause significant structural perturbation in the peptide systems. Besides of being small, the SC groups have their vibration frequency in a unique open-window (2100−2660 cm^{-1}) and do not interfere with native IR signature of peptides either. However, it should be mentioned that experimentally some combinational bands resulting from low-frequency modes may appear in this spectral window of the SC modes, which may complicate data interpretation. Nevertheless, with the introduction of the SC groups, a collection of new 2D IR cross peaks can be observed. Because of this, such SC groups may serve as structural chromophores superior to other types of site-specific labeling. Furthermore, the introduced SC modes can be of high structural specificity, while in native peptides delocalized normal modes prevail.

Acknowledgment. The authors are grateful for support from the National Natural Science Foundation of China under Grants 20773136 and 30870591, and from the National High-Tech Research and Development Program of China (863 Program) under Grants 2007AA02Z139, and the Chinese Academy of Sciences through the Hundred Talent Fund.

References and Notes

(1) Döring, V.; Mootz, H. D.; Nangle, L. A.; Hendrickson, T. L.; de Crécy-Lagard, V.; Schimmel, P.; Marlière, P. *Science* **2001**, *292*, 501.
(2) Zuend, S. J.; Coughlin, M. P.; Lalonde, M. P.; Jacobsen, E. N. *Nature* **2009**, *461*, 968.
(3) Kiick, K. L. S., E.; Tirrell, D. A.; Bertozzi, C. R. *Proc. Natl. Acad. Sci. U.S.A.* **2002**, *99*, 19.
(4) Getahun, Z.; Huang, C.-Y.; Wang, T.; De Leon, B.; DeGrado, W. F.; Gai, F. *J. Am. Chem. Soc.* **2002**, *125*, 405.
(5) Fafarman, A. T.; Webb, L. J.; Chuang, J. I.; Boxer, S. G. *J. Am. Chem. Soc.* **2006**, *128*, 13356.
(6) Yoder, N. C.; Kumar, K. *Chem. Soc. Rev.* **2002**, *31*, 335.
(7) Hohsaka, T.; Ashizuka, Y.; Murakami, H.; Sisido, M. *Nucleic Acids Res.* **2001**, *29*, 3646.
(8) Liu, W.; Brock, A.; Chen, S.; Chen, S.; Schultz, P. G. *Nat. Methods* **2007**, *4*, 239.
(9) Kwon, I.; Kirshenbaum, K.; Tirrell, D. A. *J. Am. Chem. Soc.* **2003**, *125*, 7512.
(10) Summerer, D.; Chen, S.; Wu, N.; Deiters, A.; Chin, J. W.; Schultz, P. G. *Proc. Natl. Acad. Sci. U.S.A.* **2006**, *103*, 9785.
(11) Watson, M. D.; Gai, X. S.; Gillies, A. T.; Brewer, S. H.; Fenlon, E. E. *J. Phys. Chem. B* **2008**, *112*, 13188.
(12) Ghosh, A.; Remorino, A.; Tucker, M. J.; Hochstrasser, R. M. *Chem. Phys. Lett.* **2009**, *469*, 325.
(13) Oh, K.-I.; Choi, J.-H.; Lee, J.-H.; Han, J.-B.; Lee, H.; Cho, M. *J. Chem. Phys.* **2008**, *128*, 154504.
(14) Tucker, M. J.; Kim, Y. S.; Hochstrasser, R. M. *Chem. Phys. Lett.* **2009**, *470*, 80.
(15) Asplund, M. C.; Zanni, M. T.; Hochstrasser, R. M. *Proc. Natl. Acad. Sci. U.S.A.* **2000**, *97*, 8219.
(16) Zanni, M. T.; Hochstrasser, R. M. *Curr. Opin. Struct. Biol.* **2001**, *11*, 516.
(17) Ge, N.-H.; Hochstrasser, R. M. *PhysChemComm* 2002 No 3.
(18) Khalil, M.; Demirdoeven, N.; Tokmakoff, A. *J. Phys. Chem. A* **2003**, *107*, 5258.
(19) Asbury, J. B.; Steinel, T.; Stromberg, C.; Corcelli, S. A.; Lawrence, C. P.; Skinner, J. L.; Fayer, M. D. *J. Phys. Chem. A* **2004**, *108*, 1107.
(20) Hochstrasser, R. M. *Adv. Chem. Phys.* **2006**, *132*, 1.
(21) Zhuang, W.; Abramavicius, D.; Hayashi, T.; Mukamel, S. *J. Phys. Chem. B* **2006**, *110*, 3362.
(22) Wang, J.; Chen, J.; Hochstrasser, R. M. *J. Phys. Chem. B* **2006**, *110*, 7545.
(23) DeFlores, L. P.; Tokmakoff, A. *J. Am. Chem. Soc.* **2006**, *128*, 16520.
(24) Kim, Y. S.; Liu, L.; Axelsen, P. H.; Hochstrasser, R. M. *Proc. Natl. Acad. Sci. U.S.A.* **2008**, *105*, 7720.
(25) Maekawa, H.; Toniolo, C.; Broxterman, Q. B.; Ge, N.-H. *J. Phys. Chem. B* **2007**, *111*, 3222.
(26) Strasfeld, D. B.; Ling, Y. L.; Shim, S.-H.; Zanni, M. T. *J. Am. Chem. Soc.* **2008**, *130*, 6698.

(27) Bagchi, S.; Falvo, C.; Mukamel, S.; Hochstrasser, R. M. *J. Phys. Chem. B* **2009**, *113*, 11260.
(28) Wang, J. *J. Phys. Chem. B* **2007**, *111*, 9193.
(29) Hamm, P.; Lim, M.; DeGrado, W. F.; Hochstrasser, R. M. *Proc. Natl. Acad. Sci. U.S.A.* **1999**, *96*, 2036.
(30) Decatur, S. M.; Antonic, J. *J. Am. Chem. Soc.* **1999**, *121*, 11914.
(31) Huang, C.-Y.; Getahun, Z.; Wang, T.; DeGrado, W. F.; Gai, F. *J. Am. Chem. Soc.* **2001**, *123*, 12111.
(32) Huang, R.; Kubelka, J.; Barber-Armstrong, W.; Silva, R. A. G. D.; Decatur, S. M.; Keiderling, T. A. *J. Am. Chem. Soc.* **2004**, *126*, 2346.
(33) Fang, C.; Wang, J.; Kim, Y. S.; Charnley, A. K.; Barber-Armstrong, W.; Smith, A. B., III; Decatur, S. M.; Hochstrasser, R. M. *J. Phys. Chem. B* **2004**, *108*, 10415.
(34) Petsko, G. A.; Ringe, D. *Protein Stucture and Function*, 1st ed.; New Science Press, Ltd.: London, 2003.
(35) Frisch, M. J. ; Trucks, G. W. ; Schlegel, H. B.; Scuseria, G. E.; Robb, M. A.; Cheeseman, J. R.; Vreven, J. T.; Kudin; K. N. Burant; J. C. Millam; J. M. Iyengar; S. S. Tomasi; J. Barone; V. Mennucci; B. Cossi; M. Scalmani; G. Rega; N. Petersson; G. A. Nakatsuji; H. Hada; M. Ehara; M. Toyota; K. Fukuda; R. Hasegawa; J. Ishida; M. Nakajima; T. Honda; Y. Kitao; O. Nakai; H. Klene; M. Li; X. Knox; J. E. Hratchian; H. P. Cross; J. B. Adamo; C. Jaramillo; J. Gomperts; R. Stratmann; R. E. Yazyev; O. Austin; A. J. Cammi; R. Pomelli; C. Ochterski; J. W. Ayala; P. Y. Morokuma; K. Voth; G. A. Salvador; P. Dannenberg; J. J. Zakrzewski; V. G. Dapprich; S. Daniels; A. D. Strain; M. C. Farkas; O. Malick; D. K. Rabuck; A. D. Raghavachari; K. Foresman; J. B. Ortiz; J. V. Cui; Q. Baboul; A. G. Clifford; S. Cioslowski; J. Stefanov; B. B. Liu, G. Liashenko; A.; Piskorz; P. Komaromi; I. Martin; R. L. Fox; D. J. Keith; T. Al-Laham; M. A. Peng; C. Y. Nanayakkara; A. Challacombe; M. Gill; P. M. W. Johnson; B. Chen; W. Wong; M. W. Gonzalez; C. Pople, J. A. *Gaussian 03*, Revision B.05; Gaussian, Inc.: Pittsburgh, PA, 2003.
(36) Barone, V. *J. Chem. Phys.* **2004**, *122*, 014108.
(37) Wang, J.; Hochstrasser, R. M. *J. Phys. Chem. B* **2006**, *110*, 3798.
(38) Krimm, S.; Bandekar, J. *Adv. Protein Chem.* **1986**, *38*, 181.
(39) Zanni, M. T.; Ge, N.-H.; Kim, Y. S.; Hochstrasser, R. M. *Proc. Natl. Acad. Sci. U.S.A.* **2001**, *98*, 11265.
(40) Califano, S. *Vibrational states*; John Wiley and Sons: London, 1976.
(41) Wang, J. *Phys. Chem. Chem. Phys.* **2009**, *11*, 5310.
(42) Ge, N.-H.; Zanni, M. T.; Hochstrasser, R. M. *J. Phys. Chem. A* **2002**, *106*, 962.
(43) Kuo, C. H.; Vorobyev, D. Y.; Chen, J.; Hochstrasser, R. M. *J. Phys. Chem. B* **2007**, *111*, 14028.
(44) Rubtsov, I. V.; Wang, J.; Hochstrasser Robin, M. *Proc. Natl. Acad. Sci. U.S.A.* **2003**, *100*, 5601.
(45) Londergan, C.; Wang, J.; Axelsen, P. H.; Hochstrasser, R. M. *Biophys. J.* **2006**, *90*, 4672.
(46) Anfinsen, C. B.; Edsall, J. T.; Richards, F. M. *Advances in Protein Chemistry*; Academic Press: New York, 1995.
(47) Fabian, H.; Yuan, T.; Vogel, H. J.; Mantsch, H. H. *Eur. Biophys. J.* **1996**, *24*, 195.

JP912062C